



# Coupled analysis of floating production systems

D.L. Garrett\*

*Stress Engineering Services, 13800 Westfair East Drive, Houston, TX 77041-1101, USA*

Available online 28 January 2005

## Abstract

Fully coupled global analysis of Floating Production Systems, including the vessel, the mooring system and the riser system is described. Design of the system can be a daunting task, involving more than 1000 load cases for global analysis. The primary driver for the mooring system and for the riser system is motion of the vessel. Vessel motions are driven by environmental forces, but are restrained by forces from the mooring and riser systems. Numerical models and procedures that provide accurate and efficient global modeling of the Floating Production System are presented. Both Time Domain and Frequency Domain procedures are included. The accuracy and efficiency of the procedures are illustrated in an example: a large semi with 16 mooring lines and 20 risers. The procedures provide the accuracy and efficiency for use of fully coupled analysis in design of Floating Production Systems from concept selection to final design, installation and operation.

© 2004 Elsevier Ltd. All rights reserved.

*Keywords:* Coupled; Analysis; Mooring; Risers; Dynamic; Vessel; Motion; Floating; Production

## 1. Introduction

The need for coupled analysis has long been recognized (Paulling and Webster, 1986). More recently, a number of coupled analysis tools have been introduced e.g. (Chakrabarti et al., 1996; Ormberg and Larsen, 1998; Ma et al., 2000; Colby et al., 2000; Heurtier et al., 2001; Senra et al., 2002; Correa et al., 2002; Garrett et al., 2002a).

With the exception of Stress Engineering Services' RAMS (Garrett et al., 2002a) and Shell's COSMOS (Schott et al., 1994; Phifer et al., 1994) programs, all of these coupled analysis tools are limited to the time domain. Both RAMS and COSMOS have the ability to solve the coupled problem in either the frequency or time domain.

\* Tel.: +1 281 955 2900; fax: +1 281 955 2638.

E-mail address: [david.garrett@stress.com](mailto:david.garrett@stress.com)

The computational effort required by time domain simulation led to development of frequency domain procedures for the coupled analysis. A key part of the development was an accurate and efficient method for statistical linearization of velocity-squared drag (Rodenbusch et al., 1986). An accurate and efficient finite element model for mooring lines, risers and tendons, was developed (Garrett, 1982; 1992; Paulling and Webster, 1986). The frequency domain procedures made coupled analysis for design practical (Schott et al., 1994).

The subject of this paper is the numerical modeling to allow accurate and efficient global analysis of Floating Production Systems. Modeling of the vessel, mooring lines, risers, and the links connecting the vessel to the mooring lines and risers are included. A companion paper provides an example that illustrates use of the analysis in design of mooring and riser systems for an FPSO (Garrett et al., 2003).

## 2. Models

### 2.1. Rigid body model

A Floating Production System has three types of components: (1) the vessel, modeled as a rigid body, (2) mooring lines and risers, modeled as slender elastic rods, and (3) connecting links.

The motions of a rigid body may be described in terms of the position of a reference point and three Euler angles. The position of a point,  $\mathbf{P}$ , fixed to the rigid body is

$$\mathbf{P} = \mathbf{X} + \mathbf{R}\mathbf{p} \text{ in vector notation, or } P_i = X_i + R_{ij}p_j \text{ in subscript notation} \quad (1)$$

where  $\mathbf{X}$  is the reference position of the rigid body in global coordinates;

$\mathbf{p}$  is a point on the rigid body in body-fixed coordinates;

$\mathbf{P}$  is the point  $\mathbf{p}$  in Global Coordinates;

$\mathbf{R}$  is an orthogonal transformation defined by the Euler angles.

Kinematics of the rigid body elements includes finite displacement and rotation. The orthogonal transformation representing the rotation may be written as

$$\mathbf{R} = \mathbf{R}_\phi \mathbf{R}_\theta \mathbf{R}_\psi \quad [\mathbf{R}_\phi] = \begin{bmatrix} 1 & 0 & 0 \\ 0 & \cos(\phi) & -\sin(\phi) \\ 0 & \sin(\phi) & \cos(\phi) \end{bmatrix} \quad (2)$$

$$[\mathbf{R}_\theta] = \begin{bmatrix} \cos(\theta) & 0 & \sin(\theta) \\ 0 & 1 & 0 \\ -\sin(\theta) & 0 & \cos(\theta) \end{bmatrix} \quad [\mathbf{R}_\psi] = \begin{bmatrix} \cos(\psi) & -\sin(\psi) & 0 \\ \sin(\psi) & \cos(\psi) & 0 \\ 0 & 0 & 1 \end{bmatrix}$$

For small angles, the Euler angles represent roll, pitch and yaw. The six degrees of freedom of the rigid body are the position of the reference point and the three Euler angles.

Generalized force and stiffness calculations use the position and derivatives thereof. Consider a force,  $\mathbf{F}$ , acting on the rigid body at point  $\mathbf{P}$ . The generalized force,  $\mathbf{Q}$ , and stiffness,  $\mathbf{K}$ , may be written

$$\mathbf{Q} = \mathbf{F} \cdot \frac{\partial \mathbf{P}}{\partial \mathbf{x}} \quad \mathbf{K} = -\frac{\partial \mathbf{Q}}{\partial \mathbf{x}} = -\frac{\partial \mathbf{F}}{\partial \mathbf{x}} \cdot \frac{\partial \mathbf{P}}{\partial \mathbf{x}} - \mathbf{F} \cdot \frac{\partial^2 \mathbf{P}}{\partial \mathbf{x}^2} \quad \{\mathbf{x}\} = \{X, Y, Z, \phi, \theta, \psi\}^T \quad (3)$$

The second derivative terms are retained even for small angles to provide a consistent linearization. For example, the weight of a vessel is treated as a point force acting at the center of gravity. The second derivative term is the contribution of weight to the hydrostatic stiffness. The second derivative terms are only non-zero for the Euler angle degrees of freedom.

For dynamic analysis, the vessel is usually modeled as a large volume rigid body with small dynamic motions. First and second order wave force coefficients are calculated using a radiation/diffraction program such as WAMIT (Korsmeyer et al., 1988). It is worth noting that the wave force coefficients depend only on the geometry of the wetted portion of the hull. Mean drift forces can be calculated from the wave spectrum and the second order wave force coefficients. Slow drift dynamic forces can be calculated using Newman’s approximation. A useful description of the calculation can be found in Faltinsen (1990).

Wind and current forces are usually described in terms of experimentally determined wind and current force coefficients. Wind speed has mean and slowly varying components. The slowly varying component is described by a suitable spectrum.

Mean environmental loading on the large volume rigid body does not depend on the motion of the body. Therefore, the loads can be calculated external to the Global Analysis program. For vessels that operate at varying draft, environmental load models are developed for each draft considered in the Global Analysis. Calculation of the wave force coefficients can require a significant computational effort. However, since the calculations only need be performed once for each draft, there is not a major impact on the total Global Analysis computational effort. The emphasis for wave force calculations is accuracy (Garrett et al., 2002a).

### 2.2. Elastic rod model

Mooring lines and risers are modeled using a finite element representation of an elastic rod (Garrett, 1982; 1992). The original development was for dynamics of pipelines and pipelay vessels. A portion of the derivation is included here for clarity.

The equations of motion for the elastic rod can be written

$$-(B\mathbf{r}''')' + (\lambda\mathbf{r}')' + \mathbf{q} = \rho\ddot{\mathbf{r}} \quad \frac{1}{2}(\mathbf{r}' \cdot \mathbf{r}' - 1) = \frac{T - T_0}{AE} \quad (4)$$

where  $B$  is the bending stiffness ( $EI$ );

- $\mathbf{r}(s,t)$  is the centerline of the rod;
- $\lambda = T - B\mathbf{r}'' \cdot \mathbf{r}''$  is a Lagrange multiplier;

$\mathbf{q}$  is the applied load (weight, drag, etc.);  
 $\rho$  is the mass of the rod per unit length;  
 $T$  is the tension and  $T_0$  is the unstretched tension;  
 $AE$  is the axial stiffness.

A prime denotes differentiation with respect to arclength,  $s$ , and a superposed dot denotes differentiation with respect to time. The finite element model can be developed using Galerkin’s method. The equation may be written

$$\int_0^L [-B\mathbf{r}'' \cdot \delta\mathbf{r}'' - \lambda\mathbf{r}' \cdot \delta\mathbf{r}' + (\mathbf{q} - \rho\ddot{\mathbf{r}}) \cdot \delta\mathbf{r}] ds = (\mathbf{r}' \times \mathbf{M}) \cdot \delta\mathbf{r}'|_0^L - \mathbf{F} \cdot \delta\mathbf{r}|_0^L \tag{5}$$

where  $\mathbf{M}$  is the bending moment,  $\mathbf{F}$  is the force (tension and shear) and  $\delta$  denotes the variation. The centerline  $\mathbf{r}$  is interpolated using cubic Hermetian shape functions and the Lagrange multiplier is interpolated using quadratic shape functions. The element has 15 degrees of freedom. The force and moment at each end of the element are determined from the integral. For internal nodes, the integral provides two independent estimates of force and moment from the elements on either side of the node. The residual from the two estimates provides a measure of error.

The equation for axial stretch may be written

$$\int_0^L \frac{1}{2}(\mathbf{r}' \cdot \mathbf{r}' - 1)\delta\lambda \, ds = \int_0^L \frac{T - T_0}{AE} \delta\lambda \, ds \tag{6}$$

For numerical implementation, the distinction between  $\lambda$  and  $T$  is dropped, since

$$\frac{\lambda}{AE} = \frac{T}{AE} + O(\varepsilon_b^2) \tag{7}$$

where  $\varepsilon_b$  is the bending strain.

With this formulation, the Lagrange multipliers can be eliminated at the element level, leaving 6 degrees of freedom per node. The equations are banded with a bandwidth of 12. Linear variation of bending stiffness is included to provide efficient modeling of tapered stress joints.

The element stiffness and mass matrices can be assembled using a set of constant arrays, similar to a small angle, linear, tensioned beam element. Direct wave and current loads are described using a Morison formulation (Rodenbusch et al., 1986)

$$\mathbf{q} = C_d\mathbf{V}_n|\mathbf{V}_n| + C_m\mathbf{a}_n - C_a\ddot{\mathbf{r}}_n \tag{8}$$

where  $C_d$ ,  $C_m$ , and  $C_a$  are the drag, inertia and added mass coefficients,  $\mathbf{V}_n$  is the normal component of relative velocity,  $\mathbf{a}_n$  is the normal component of water particle acceleration, and  $\ddot{\mathbf{r}}_n$  is the normal component of the rod acceleration.

Distributed drag and wave acceleration loads are integrated using six point Gaussian quadrature. The added mass matrix is integrated exactly and uses constant arrays for assembly. For Frequency Domain calculation, the drag load is replaced by the linear relative velocity drag calculated using statistical linearization (Rodenbusch et al., 1986). The damping matrix is of the same form as the added mass matrix.

The formulation presented provides a consistent and accurate representation of the Jacobian of internal forces, which is essential for robustness in static and dynamic analysis. Convergence is ensured due to the direct attack of the exact equations of motion. Extension of the element to include torque (axial component of moment) is straightforward (Mullarkey and McNamara, 2000). However, the number of element degrees of freedom increases to 27. Torque is relatively unimportant for mooring lines and risers in Floating Production Systems. Other element formulations that use approximations to the Jacobian (O'Brien et al., 2002) can require more elements and smaller time steps.

### 2.3. Connecting link models

Connecting links between the rod element models and the rigid body models are in the form of extensional and rotational springs. Consider an extensional spring with the potential energy function

$$V = \frac{1}{2}K(\mathbf{P}_1 - \mathbf{P}_2) \cdot (\mathbf{P}_1 - \mathbf{P}_2) \quad (9)$$

where  $\mathbf{P}_1$ ,  $\mathbf{P}_2$  are points defining the 'ends' of the spring and  $K$  is the spring constant.

An end of the spring can be a location in a rod element, a location on a rigid body, or a point in the global coordinate system. A stiff spring can represent a pinned connection.

The potential energy in a rotational spring can be written

$$V = \frac{1}{2}K_r \left( \frac{\mathbf{E}_1}{|\mathbf{E}_1|} - \frac{\mathbf{E}_2}{|\mathbf{E}_2|} \right) \cdot \left( \frac{\mathbf{E}_1}{|\mathbf{E}_1|} - \frac{\mathbf{E}_2}{|\mathbf{E}_2|} \right) \quad (10)$$

where  $\mathbf{E}_1$ ,  $\mathbf{E}_2$  are directions and  $K_r$  is the rotational spring constant.

The directions can be the tangent to the rod element centerline, a fixed direction in rigid body local coordinates or a fixed direction in global coordinates. A stiff rotational spring can represent a clamped constraint. A finite stiffness spring can represent a flex joint. Since each node in the rod element has six degrees of freedom and each rigid body has six degrees of freedom, 12 generalized forces and a  $12 \times 12$  stiffness matrix are generated for each spring. The generalized forces,  $\mathbf{Q}$ , and stiffness,  $\mathbf{K}$ , are defined by

$$\mathbf{Q} = -\frac{\partial V}{\partial \mathbf{x}}; \quad \mathbf{K} = -\frac{\partial \mathbf{Q}}{\partial \mathbf{x}} \quad (11)$$

where  $\mathbf{x}$  can include rod element or rigid body degrees of freedom. Other forms can be used to model tensioners, lateral guides, etc. The vertical restraint of the seafloor is modeled as a discontinuous quadratic spring with eight or more discrete springs distributed uniformly within an element. All force models should have continuous first partial derivatives so the Jacobian is well defined. The complete Jacobian should be included for robustness in static and dynamic analysis.

### 3. Time domain procedures

The second order equations of motion for the discrete model are reduced to two first order equations and integrated using the trapezoidal rule as described in Garrett (1982). Some implementation aspects are summarized here. The equations of motions may be written

$$\mathbf{M}\ddot{\mathbf{y}} = \mathbf{Q} \quad \text{or} \quad \mathbf{M}\dot{\mathbf{z}} = \mathbf{Q} \quad \dot{\mathbf{y}} = \mathbf{z} \quad (12)$$

For numerical integration, the first order equations are written in discrete form

$$\mathbf{M}\left(\frac{\mathbf{z}_{n+1} - \mathbf{z}_n}{h}\right) = \frac{1}{2}(\mathbf{Q}_n + \mathbf{Q}_{n+1}) \quad \frac{\mathbf{y}_{n+1} - \mathbf{y}_n}{h} = \frac{1}{2}(\mathbf{z}_n + \mathbf{z}_{n+1}) \quad (13)$$

where  $n$  is the step and  $h$  is the time step. The equations may be solved with Newton's method or other iteration. The complete Jacobian of some of the force terms is not easily calculated. For implementation, the generalized forces may be written

$$\mathbf{Q} = \mathbf{F} + \mathbf{H} \quad (14)$$

where  $\mathbf{H}$  is the hydrodynamic load and  $\mathbf{F}$  includes internal loads and external loads for which derivatives are available.  $\mathbf{F}$  may be expanded as

$$\mathbf{F}_{n+1} \approx \mathbf{F}_n - \mathbf{K}(\mathbf{y}_{n+1} - \mathbf{y}_n) \quad (15)$$

The discrete equations become

$$\begin{aligned} \mathbf{M}\left(\frac{\mathbf{z}_{n+1} - \mathbf{z}_n}{h}\right) &= \frac{1}{2}(2\mathbf{F}_n - \mathbf{K}(\mathbf{y}_{n+1} - \mathbf{y}_n)) + \frac{1}{2}(3\mathbf{H}_n - \mathbf{H}_{n-1}) \frac{\mathbf{y}_{n+1} - \mathbf{y}_n}{h} \\ &= \frac{1}{2}(\mathbf{z}_n + \mathbf{z}_{n+1}) \end{aligned} \quad (16)$$

The hydrodynamic loads, including radiation terms, are integrated using the explicit Adams–Bashforth method and the forces for which derivatives are available are included implicitly. The equations may be rearranged for solution as described in Garrett (1982). One calculation per time step is required (no iteration). A constant time step is recommended.

### 4. Frequency domain procedures

Solution in the Frequency Domain involves solution of a nonlinear statics problem and a set of linear harmonic load cases. The solution assumes stationary response. Stiffness coefficients are calculated at the mean position and velocity-squared drag linearization is based on the current estimate of relative velocity statistics (Rodenbusch et al., 1986). Mean forces and linearization coefficients depend on response statistics, so the procedure is iterative. The equations of motion may be written

$$\mathbf{M}\ddot{\mathbf{Y}} = \mathbf{F} + \mathbf{H} \quad (17)$$

For Frequency Domain analysis, the forces and responses are assumed to be a linear sum of harmonic components

$$\begin{aligned}\mathbf{Y} &= \sum_{n=0}^N \mathbf{y}_n \exp(-i\omega_n t) = \bar{\mathbf{y}} + \sum_{n=1}^N \mathbf{y}_n \exp(-i\omega_n t) \\ \mathbf{F} &= \sum_{n=0}^N \mathbf{f}_n \exp(-i\omega_n t) = \bar{\mathbf{f}} + \sum_{n=1}^N \mathbf{f}_n \exp(-i\omega_n t) \\ \mathbf{H} &= \sum_{n=0}^N \mathbf{h}_n \exp(-i\omega_n t) = \bar{\mathbf{h}} + \sum_{n=1}^N \mathbf{h}_n \exp(-i\omega_n t)\end{aligned}\quad (18)$$

The means are real and the component amplitudes are complex. The dynamic forces are represented by linear components as

$$\mathbf{f} = \bar{\mathbf{f}} - (\mathbf{K} - i\omega\mathbf{C}) \sum \mathbf{y}_n \exp(-i\omega_n t) \quad (19)$$

where the stiffness,  $\mathbf{K}$ , and the damping,  $\mathbf{C}$ , are calculated at the mean position using current estimates of response statistics. Since first order wave forces, slow drift forces and wind forces are statistically independent, the frequencies used for analysis are separated into three parts (wave frequency, slow drift and wind). For the wave frequency components, the frequency dependent added mass vessel coefficients are used. The zero frequency added mass is used for wind and slow drift frequency components. The iterative procedure for the linearization coefficients is direct, so under-relaxation is employed to ensure convergence.

## 5. Example

The procedures described have been implemented in Rational Approach to Marine Systems (RAMS). Time Domain and Frequency Domain solvers are included in the same code. The same data is used in both Time Domain and Frequency Domain simulations. Frequency Domain simulations assume stochastic and stationary response. Time Domain simulations can include transient or stationary cases.

Application of the procedures is illustrated by an example: a large semi-submersible platform moored in 1800 m water depth in the Gulf of Mexico. The vessel is moored with a semi-taut, chain-wire-chain, system arranged in a  $4 \times 4$  pattern. Twenty Steel Catenary Risers (SCRs) are arranged in four groups of five, with attachment points at pontoon level. The system is shown in Fig. 1. The vessel has two planes of symmetry; particulars are in Table 1. Mooring line properties are in Table 2. SCR properties are in Table 3.

Element lengths were chosen using the procedures in Garrett et al. (2002a). The models are sufficiently detailed for fatigue analysis. The total number of rod elements is 3554 and the number of degrees of freedom is 21,546. More detail is in Table 4. The model size is typical of deep water Floating Production Systems. Systems with 100,000 degrees of freedom can be solved completely in random access memory on a PC with 512 MB of RAM.

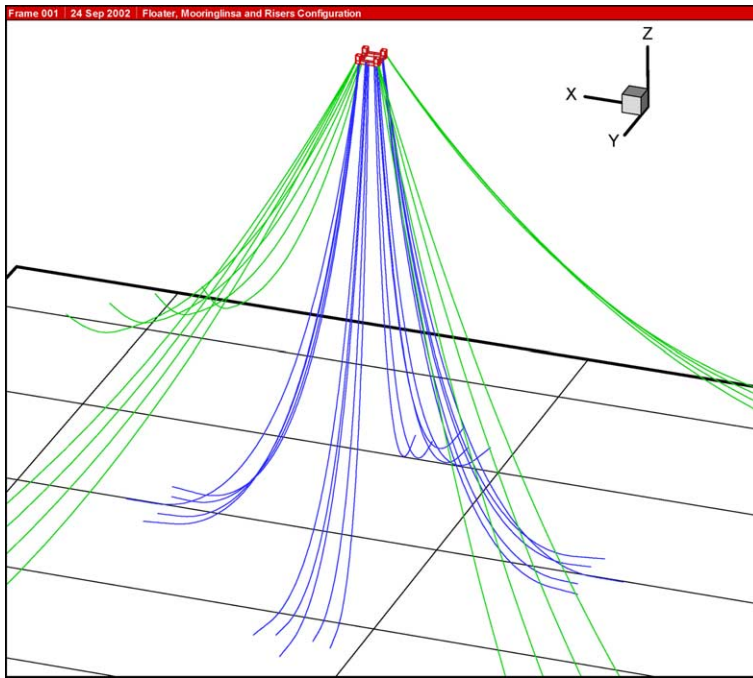


Fig. 1. Large semi with 16 mooring lines and 20 risers.

A moderate sea state with a significant wave height of 3 m was selected for comparison of Time Domain and Frequency Domain simulation. The sea state is the most damaging sea state in the fatigue scatter diagram. The wave, wind and current are from vessel South. The simulation parameters in Table 5 were selected using the procedures in Garrett et al.

Table 1  
Vessel dimensions

Columns (square): centerline spacing (m)	64
Width (m)	17.2
Pontoons (rectangular): height (m)	10.5
Width (m)	12.4
Draft (m)	27.5
Displacement (tonnes)	58,122

Table 2  
Mooring line data

Segment	Diameter (mm)	Length (m)
Platform chain	124	61
Spiral strand	114	2316
Ground chain	114	335

Table 3  
SCR properties

Parameter	Water injection	Oil	Gas
Diameter (mm)	219	219	270
Wall thickness (mm)	14.3	14.3	14.3
Insulation OD (mm)	–	371	–
Insulation density (kg/m <sup>3</sup> )	–	721	–
Contents density (kg/m <sup>3</sup> )	1025	480	160
Departure angle (°)	6.3	6.3	7.6

Table 4  
Model size

No. of riser elements	3170
No. of mooring elements	384
Total number of elements	3554
Total degrees of freedom	21,546

(2002a). The large number of frequencies used was based on Time Domain simulation requirements; Frequency Domain Analysis could use approximately one fifth as many components.

Variance of Surge, Heave and Pitch motions are compared in Fig. 2. The ratio of the Time Domain result for each replicate to the Frequency Domain result (one value) is shown. Surge motion shows the most variability, which is expected due to the long surge period (about 250 s). The spectral moments of the results are statistically indistinguishable. Comparisons were made using the procedures in Garrett et al. (2002a).

The stress variance for the Gas SCR on the North pontoon is shown in Fig. 3. The Time Domain result is the average of the 10 replicates. The peak at the left is near the touchdown point for the SCR. The peak at the right is at the hangoff location. A closer look at the touchdown point is shown in Fig. 4. Individual replicates are plotted, together with the Frequency Domain result. A similar comparison near the stress joint at the top of the riser

Table 5  
Simulation parameters for fully coupled comparison

Significant wave height, $H_s$ (m)	3
Peak period, $T_p$ (s)	8.1
Wind speed (m/s)	12.3
Current speed (m/s)	0.37
Transient (s)	2000
Simulation (s)	3600
Replicates	10
Wave frequencies	899
Wind frequencies	470
Slow drift frequencies	470
Total frequencies	1839
Time step (s)	0.1

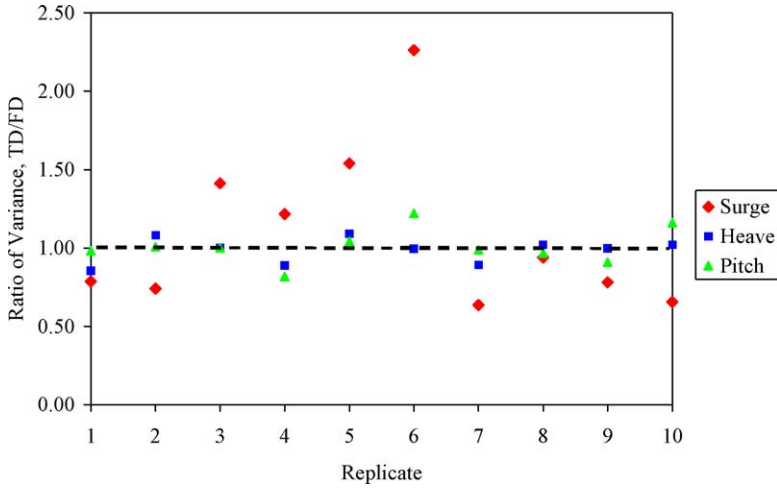


Fig. 2. Vessel motion variance comparison.

is shown in Fig. 5. Variance of mooring line tension for the most loaded line is shown in Fig. 6. The vessel motion, SCR stress and mooring line tension calculated in the Time Domain are statistically indistinguishable from the Frequency Domain result.

The test case provides an illustration of the accuracy and efficiency provided by the Frequency Domain procedures. The Frequency Domain simulation required approximately 15 min on a 1.8 GHz PC. The Time Domain simulation required approximately 100 h (for the 10 replicates) on the same PC. The Frequency Domain and Time Domain simulation results are equivalent. Frequency Domain simulation requires fewer frequency

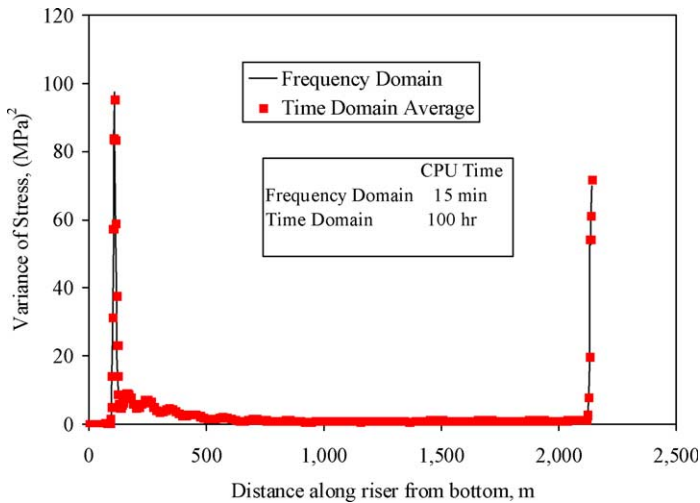


Fig. 3. Variance of stress in gas SCR.

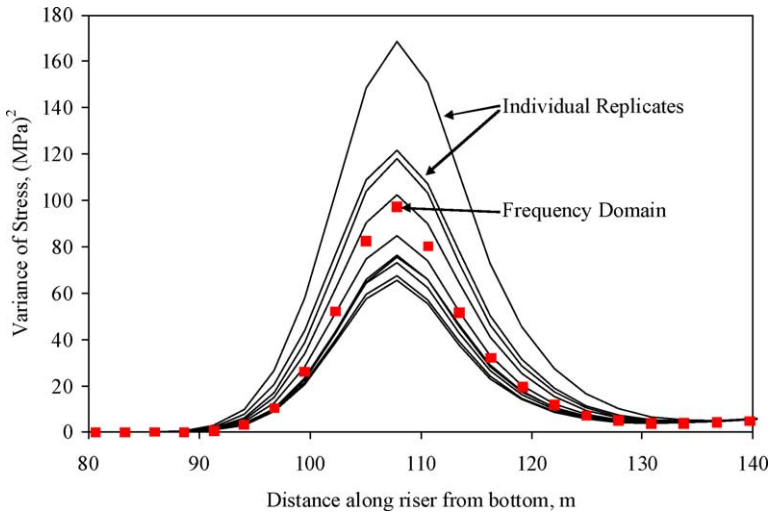


Fig. 4. Stress variance near touchdown—gas riser.

components than Time Domain simulation (Garrett et al., 2002a). Thus, the Frequency Domain computational advantage is greater than the 400–1 ratio for this example. Frequency Domain simulation requires about three orders of magnitude less computation than Time Domain simulation to produce equivalent results.

The excellent match of low frequency motions of the vessel demonstrates the effectiveness of the statistical linearization procedure in capturing damping due to drag on the mooring lines and risers. This is not surprising, since the linearization procedure matches the energy dissipated by drag (Rodenbusch et al., 1986; Garrett et al., 2002b).

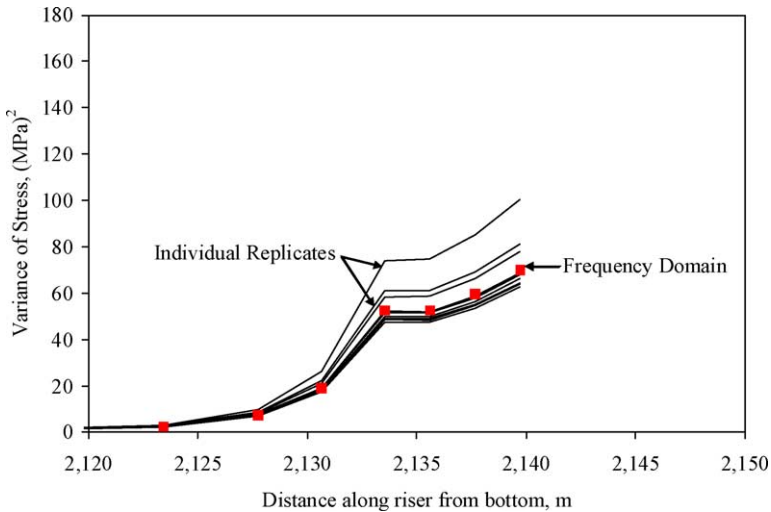


Fig. 5. Stress variance near stress joint—gas riser.

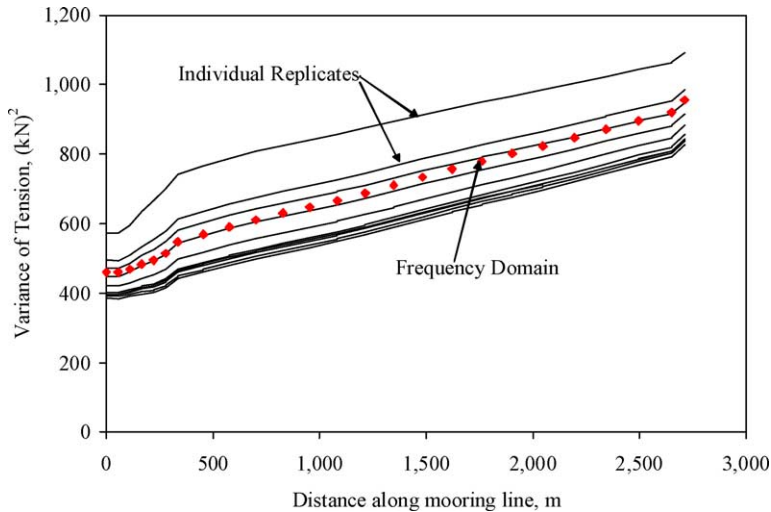


Fig. 6. Variance of mooring line tension.

The Frequency Domain and Time Domain results do not match as well for all cases. The same problem was repeated for the 100 year Hurricane load case. Simulation parameters are in Table 6. Vessel motions were calculated in the Frequency Domain. The vessel motions were used to drive the Gas SCR on the North pontoon for 10 1 h simulations. Variance of stress near the touchdown point is compared in Fig. 7. The Frequency Domain result is slightly higher than the Time Domain result. The difference is a result of the varying touchdown point that is captured in the Time Domain simulation. Application of statistical linearization to the seafloor model could bring the results closer together. A comparison of variance of stress near the stress joint is shown in Fig. 8; the agreement is quite good.

Table 6  
Simulation parameters for 100 year hurricane analysis

Significant wave height, $H_s$ (m)	12.2
Peak period, $T_p$ (s)	15
Wind speed (m/s)	41.8
Current Speed, m/sec	1.1
Transient (s)	2000
Simulation (s)	3600
Replicates, SCR	10
Replicates, mooring line	100
Wave frequencies	459
Wind Frequencies	301
Slow drift frequencies	301
Total frequencies	1061
Time step (s)	0.1

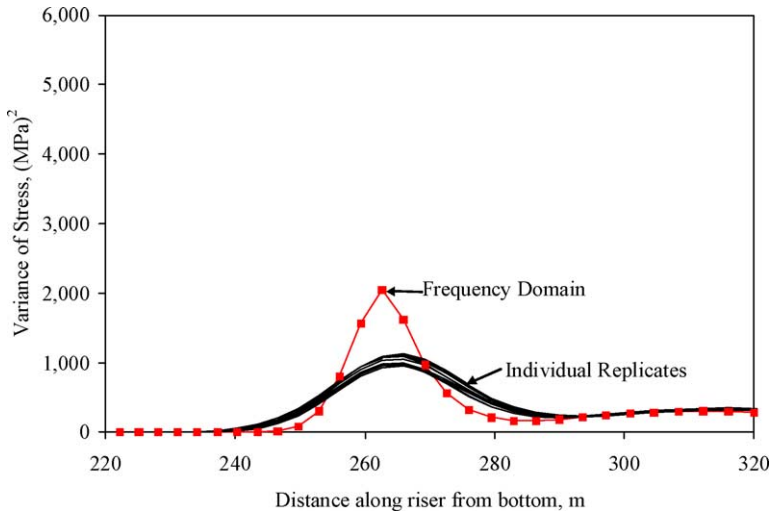


Fig. 7. Stress variance for 100 year hurricane near touchdown.

The most loaded mooring line was driven by the Frequency Domain calculated motions for 100 1 h simulations. A comparison of the first two spectral moments is shown in Fig. 9. The Time Domain and Frequency Domain results are statistically indistinguishable.

Comparisons of Time Domain and Frequency Domain simulations for top tensioned risers and mooring lines for a deep water Spar are presented in Garrett et al. (2002a). Similarly good comparisons are found. The comparisons presented are typical for deep water Floating Production Systems.

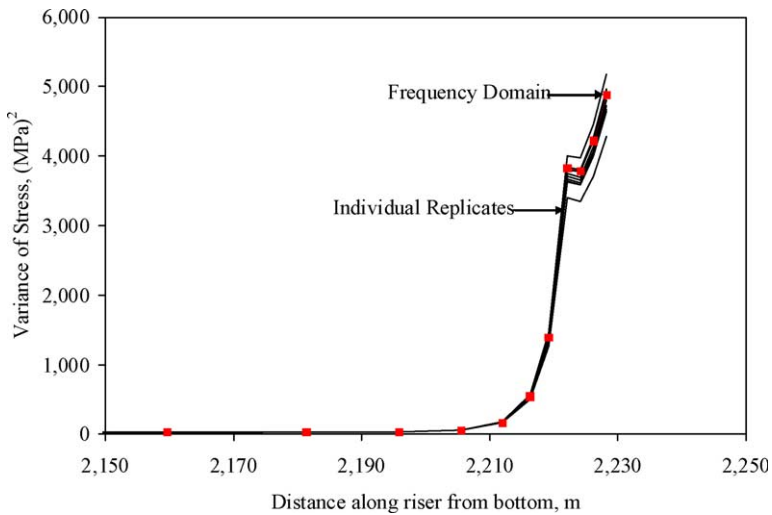


Fig. 8. Stress variance near stress joint for 100 year hurricane.

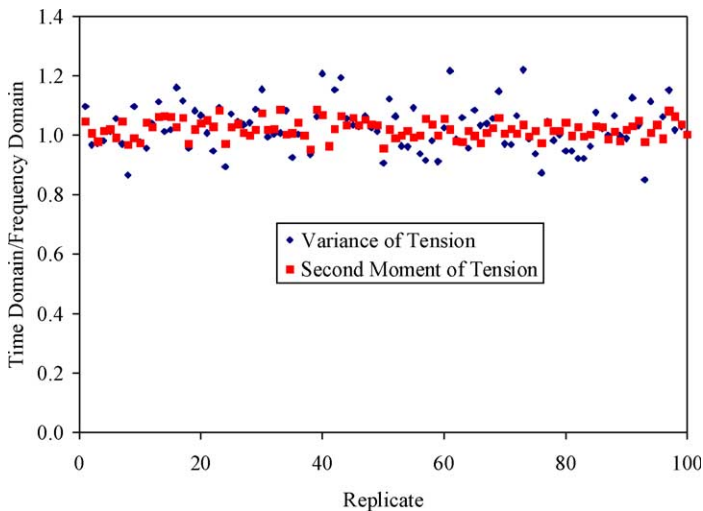


Fig. 9. Tension statistics for 100 year hurricane.

## 6. Conclusions

Computational procedures for fully coupled Time Domain and for fully coupled Frequency Domain simulation of Floating Production Systems are presented. The procedures provide the accuracy and efficiency needed for design of Floating Production Systems. Comparison of Time Domain and Frequency Domain simulations demonstrate the effectiveness of the procedures. The example demonstrates the two to three order of magnitude gain in computational efficiency using the Frequency Domain procedure with no loss of accuracy.

## References

- Chakrabarti, P., Chandwani, R., Larsen, I., 1996. Analyzing the Effect of Integrating Riser/Mooring Line Design, Proceedings of OMAE'96 1996.
- Colby C., Sodahl N., Katla E., Okkenhaug S., 2000. Coupling Effects for a Deepwater Spar. OTC 12083.
- Correa F.N., Senra S.F., Jacob B.P., Masetti I.Q., Mourelle M.M., 2002. Towards the Integration of Analysis and Design of Mooring Systems and Risers, Part II: Studies on a DICAS System. OMAE 2002-28151, Oslo.
- Faltinsen, O.M., 1990. Sea Loads on Ships and Offshore Structures. Cambridge Press, Cambridge.
- Garrett, D.L., 1982. Dynamic Analysis of Slender Rods. Journal of Energy Resources Technology. Transactions of ASME 104, 302–307.
- Garrett D.L., 1992. Structural Analysis of Marine Risers. NSF Workshop on Riser Mechanics, University of Michigan, Ann Arbor.
- Garrett D.L., Chappell J.F., Gordon R.B., 2002. Global Performance of Floating Production Systems. OTC 14230.
- Garrett D.L., Gordon R.B., Chappell J.F., 2002. Mooring- and Riser-Induced Damping in Fatigue Seastates. OMAE2002-28550, Oslo.
- Garrett, D.L., Chappell, J.F., Gordon, R.B., Cao, Y., 2003. Integrated Design of Risers and Moorings, Proceedings 2003 International Symposium on Deepwater Mooring Systems 2003.

- Heurtier, J.M., le Buhan, P., Fontaine, E., le Cunff, C., Biolley, F., Berhault, C., 2001. Coupled Dynamic Response of Moored FPSO with Risers, Proceedings of the ISOPE'01, Stavanger 2001.
- Korsmeyer, F.T., Lee, C.H., Newman, J.N., Sclavounos, P.D., 1988. The Analysis of Wave Effects on TLP, Proceedings of OMAE'88, Houston 1988.
- Ma W., Lee M.-Y., Zou J., Huang E.W., 2000. Deepwater Nonlinear Coupled Analysis Tool. OTC 12085.
- Mullarkey, T.P., McNamara, J.F., 2000. A Novel Method for the Representation of Large Scale Torque and Twist with Bending of Elastic Rods, in: O'Donoghue, P.E., Flavia, J.N. (Eds.), Proceedings of the Symposium on Trends in the Application of Mathematics to Mechanics (STAMM 2000). The Data Science Library, Paris, pp. 139–146.
- O'Brien P.J., Lane M., McNamara J.F., 2002. Improvements to the Convected Co-Ordinates Method for Predicting Large Deflection Extreme Riser Response. OMAE2002-28237, Oslo.
- Ormberg, H., Larsen, K., 1998. Coupled analysis of floater motion and mooring dynamics for a turret-moored ship. Applied Ocean Research 20, 55–67.
- Paulling, J.R., Webster, W.C., 1986. Large-amplitude analysis of the coupled response of a TLP and tendon system, Proceedings of OMAE'86, Tokyo, 86 1986.
- Phifer E.H., Koop F., Swanson R.C., Allen D.W., Langer C.G., 1994. Design and Installation of Auger Steel Catenary Risers. OTC. 7620.
- Rodenbusch, G., Garrett, D.L., Anderson, S.L., 1986. Statistical Linearization of Velocity-Squared Drag Forces, Proceedings of OMAE'86, Tokyo 1986 pp. 123–129.
- Schott W.E., Rodenbusch G., Mercier R.S., Webb C.M., 1994. Global Design and Analysis of the Auger Tension Leg Platform. OTC 7621, pp. 541–552.
- Senra S.F., Correa F.N., Jacob B.P., Mourelle M.M., Masetti I.Q., 2002. Towards the Integration of Analysis and Design of Mooring Systems and Risers, Part I: Studies on a Semisubmersible Platform. OMAE 2002-28046, Oslo.